

Research Article

Updating Soil Spatial Variability and Reducing Uncertainty in Soil Excavations by Kriging and Ensemble Kalman Filter

Yajun Li ¹ and Kang Liu²

¹School of Engineering and Technology, China University of Geosciences (Beijing), Beijing, China

²School of Civil and Hydraulic Engineering, Hefei University of Technology, Hefei, China

Correspondence should be addressed to Yajun Li; y.j.li@cugb.edu.cn

Received 16 June 2019; Revised 14 September 2019; Accepted 19 September 2019; Published 20 October 2019

Guest Editor: Young-Suk Song

Copyright © 2019 Yajun Li and Kang Liu. This is an open access article distributed under the Creative Commons Attribution License, which permits unrestricted use, distribution, and reproduction in any medium, provided the original work is properly cited.

Field measurements can be used to improve the estimation of the performance of geotechnical projects (e.g., embankment slopes and soil excavation pits). Previous research has utilised inverse analysis (e.g., the ensemble Kalman filter (EnKF)) to reduce the uncertainty of soil parameters, when measurements are related to performance, such as inflow, hydraulic head, and deformation. In addition, there are also direct measurements, such as CPT measurements, where parameters (i.e., tip resistance and sleeve friction) can be directly correlated with, e.g., soil deformation and/or strength parameters, where conditional simulation via constrained random fields can be used to improve the estimation of the spatial distribution of parameters. This paper combines these two (i.e., direct and indirect) methods together in a soil excavation analysis. The results demonstrate that the parameter uncertainty (and thereby the uncertainty in the response) can be significantly reduced when the two methods are combined.

1. Introduction

Soil properties are spatially varying due to mineralogical compositions, stress histories, and geological disposal processes [1–3]. Therefore, in a routine site investigation program where soil samples are tested at some places, soil property values at unsampled locations cannot be interpolated or extrapolated with perfect certainty (i.e., due to the spatial variability). However, it is often desirable to predict those property values (with as little uncertainty as possible) at those locations, in order to reduce the uncertainties in the soil structural responses.

Conditional random field approaches that aim to reduce the uncertainty are available to generate realisations of random fields, constrained by the direct measurement data at sampling locations. The Monte Carlo process is often involved in those approaches. Bayesian updating based on Markov Chain Monte Carlo (MCMC) can be used to generate multiple realisations of soil properties. For example, Li et al. [4] used MCMC for generating conditioned random fields of depth to bedrock in the geologic profiles.

An alternative way is to use kriging combined with an unconditional random field generator [5]. Kriging provides a best linear unbiased estimation of spatially random properties at unsampled locations, by weighing the sampled measurements according to the covariance (variogram) [6]. Multiple realisations of soil properties can also be generated to investigate the uncertainty in structure responses. For instance, Li et al. [5] used kriging to generate the random fields of undrained shear strength by using the direct cone penetration test (CPT) data.

Apart from the “direct” measurement data, monitoring data of the soil structure performance is quite often available. Conditional simulation of random fields of soil properties and of the soil structures on or around these soils can be also achieved by using these indirect soil response data and inverse modelling techniques. For example, making use of all deflection measurements along an inclinometer, Lo and Leung [7] showed that Bayesian methods can be used to update subsurface soil spatial variability in order to improve the prediction of the response of a braced excavation. Vardon et al. [8] used the ensemble Kalman filter (EnKF) to

reduce the uncertainty in slope stability based on hydraulic measurements via inverse analysis.

However, conditional simulation based on both direct and indirect measurements is surprisingly scarce in geotechnical engineering, except the study by Li et al. [4], who claimed that their approach can take account of both sources of measurement data, although they provided an explicit relationship between the response and the property of interest in their case. The relationship between the soil response and soil property, however, does not have an explicit form in most cases. Therefore, this paper presents a framework for uncertainty reduction in soil deposits with spatial variability by conditioning a random field using both direct soil property measurements and indirect soil response measurements. A numerical soil excavation example was used to demonstrate the improvement of soil property field and the soil deformation estimations during various stages of excavation. The idea is to show the efficiency of the two sources of information when used to condition the random fields of soil properties and their relative contribution to the overall uncertainty reduction in the performance.

2. RF Model: Unconditional Random Field Generation

Random fields (RF) are used for representing spatially variable soil properties, and they have found extensive use in practical geotechnical applications [9]. They are usually used in combination with the finite element method to investigate the uncertainties in the soil structure response. There are various methods of representing random fields in finite element analysis [10, 11], including: (i) midpoint or nodal point method [12], in which the field within the domain of an element is described by a single random variable representing the value of the field at a central point of the element; (ii) spatial averaging method [13], which describes the field within each element in terms of the spatial average of the field over the element; (iii) shape function method [14], which describes the random field within an element in terms of a set of nodal values and corresponding shape functions; and (iv) series expansion method, such as Karhunen–Loeve expansion, which expresses the field in terms of its spectral decomposition [15].

Classical statistical characteristics of soil properties, in the case of describing the soil properties as single variables, include the parameters defining the probability distribution of the variable, such as the mean value (μ), standard deviation (σ) or variance (σ^2), and coefficient of variation (COV) ($V = \sigma/\mu$). In the case of spatial variability, an additional parameter, the scale of fluctuation (SOF) (θ) [16], which measures the distance over which soil property values show relatively strong correlation from point to point in space, should be introduced.

The local average subdivision (LAS) method, which falls in the category of “spatial averaging”, is used in this paper to generate random field realisations of spatially varying soil properties, using the aforementioned soil statistical parameters and a certain form of spatial correlation function parametrized by SOF. In the case that the scale of fluctuation

is direction-dependent, the anisotropy of correlation distance of the soil spatial heterogeneity ($\xi = \theta_h/\theta_v$) is modelled by defining different values of SOF in the vertical and horizontal directions (i.e., θ_v and θ_h , respectively) for horizontally deposited soil mass. This has previously been reported and implemented, for example, by Hicks and Samy [17] and Hicks and Spencer [18] and Li et al. [19] in 2D and 3D, respectively.

A frequently used autocorrelation function for generating random fields is of the exponential form and is used in this study; that is,

$$\rho(\tau_1, \tau_2) = \exp\left(-\sqrt{\left(\frac{2\tau_1}{\theta_1}\right)^2 + \left(\frac{2\tau_2}{\theta_2}\right)^2}\right), \quad (1)$$

where τ is the lag distance between two points in space and subscripts 1 and 2 denote the vertical and lateral coordinate direction, respectively.

Note that the local average subdivision (LAS) algorithm itself is incapable of preserving correlation anisotropy [20]. In case an anisotropic field is desired, an isotropic random field (i.e., $\theta_1 = \theta_2$) can initially be generated, and this isotropic field can then be postprocessed to give the target anisotropic random field. That is, an anisotropic field can be obtained by squashing and/or stretching the isotropic field in the vertical and/or horizontal directions, respectively. However, due to the scarcity of data intensity in the horizontal direction, the horizontal characterization of spatial correlation is often less frequently seen in geotechnical engineering. Although evidence has shown that correlation of soil properties tends to be stronger in the horizontal direction than that in the vertical direction, this paper focuses on isotropic correlation to show the effect of conditioning. It is believed that the effect only differs in the magnitude of uncertainty reduction for an anisotropically correlated field.

3. RF Model: Conditional Random Field Generation via Kriging and EnKF

Conditional random fields using kriging and EnKF are used in this paper to investigate their effects on reducing the uncertainties of spatially varying soil parameter realisations and thereby on the uncertainty reduction of soil excavation displacements. Random fields of soil properties conditioned on direct property measurements and/or indirect response measurements via kriging and EnKF are briefly introduced here, respectively.

3.1. Generation of Conditional Random Fields via Kriging. The generation of a conditional random field involves two steps [5]: (i) generation of an unconditional random field, $\mathbf{E}_{ru}^i(\mathbf{x}) = (E_1, E_2, \dots, E_n)^T$, of the spatial variability of soil properties (where \mathbf{x} denotes a location in space, n is the number of locations representing the random field, and i denotes the realisation number); (ii) conditioning the random field, e.g., kriging estimates, \mathbf{E}_{km} , based on measured

values at $\mathbf{x}_j (j = 1, 2, \dots, N_k)$ and kriging estimates, \mathbf{E}_{ks}^i , based on unconditionally (or randomly) simulated values at the same positions $\mathbf{x}_j (j = 1, 2, \dots, N_k)$, where N_k is the number of direct measurement locations, are combined with \mathbf{E}_{ru}^i from step (i) to give the conditional random field, \mathbf{E}_{rc}^i , that is,

$$\mathbf{E}_{rc}^i(\mathbf{x}) = \mathbf{E}_{km}(\mathbf{x}) + (\mathbf{E}_{ru}^i(\mathbf{x}) - \mathbf{E}_{ks}^i(\mathbf{x})). \quad (2)$$

It is noted that the superscript i is absent in the aforementioned equation for $\mathbf{E}_{km}(\mathbf{x})$. This is because the kriging estimation based on measurements does not need to be performed for each realisation of the random field; it only needs to be performed once and it is the same for all realisations.

3.2. Generation of Conditional Random Fields via EnKF. This paper uses the method developed by the second author in an earlier study [8] and the method description partly reproduces their wording. The method is now presented in the context of a soil excavation problem for easy understanding. The EnKF method follows an iterative process, in which each iteration contains two steps: forecast and update. For applying the EnKF to stochastic soil excavation problems, a state vector has to be constructed to incorporate both unknown local deformation parameters (e.g., elastic modulus) and measurements of soil displacements. This is expressed as

$$\mathbf{Z}_i = \begin{pmatrix} \mathbf{E}^i \\ \mathbf{d}^i \end{pmatrix}, \quad (3)$$

where subscript i represents an realisation of the ensemble;

$$\mathbf{E}^i = (E_1, E_2, \dots, E_n)^T, \quad (4)$$

is the vector of normally distributed elastic modulus ($\mathbf{E}^i = \mathbf{E}_{rc}^i$ for conditional random fields based on kriging and $\mathbf{E}^i = \mathbf{E}_{ru}^i$ for unconditional random fields);

$$\mathbf{d}^i = (d_1, d_2, \dots, d_m)^T, \quad (5)$$

is the vector of displacements computed at the measurement locations; n and m are the number of unknown elastic modulus values and soil displacement measurements, respectively.

In this investigation, the number of unknown elastic modulus values is equal to the number of elements in the finite element mesh. In the EnKF, an ensemble of N state vectors is used to simulate the initial estimation of the elastic modulus field, that is,

$$\mathbf{Z} = [\mathbf{Z}_1, \mathbf{Z}_2, \dots, \mathbf{Z}_N]. \quad (6)$$

In the forecasting step of each iteration, the ensemble of state vectors is forecasted to the second (i.e., update) step by the model describing the problem (i.e., the finite element model), that is,

$$\mathbf{Z}_t = F(\mathbf{Z}_{t-1}), \quad (7)$$

where t is the iteration number in the EnKF. In this case, the soil excavation model is utilised to compute the displacements

for all realisations of the ensemble, based on the updated elastic modulus fields from the end of the previous iteration. After the forecasting step, the computed displacements at the measurement locations in the forecasted ensemble of state vectors are compared with the collected "real" displacement measurements. The ensemble of state vectors is then updated (with respect to elastic modulus) by

$$\begin{aligned} \mathbf{Z}_t^{\text{udt}} &= \mathbf{Z}_t^f + \mathbf{K}_G(\mathbf{D} - \mathbf{H}\mathbf{Z}_t^f), \\ \mathbf{D} &= [\mathbf{d}^1, \mathbf{d}^2, \dots, \mathbf{d}^N], \\ \mathbf{d}^i &= \mathbf{d}^* + \boldsymbol{\varepsilon}_i, \end{aligned} \quad (8)$$

where $\mathbf{Z}_t^{\text{udt}}$ is the matrix containing the ensemble of updated state vectors, of dimensions $(m+n) \times N$, and \mathbf{Z}_t^f is the corresponding matrix of state vectors resulting from the forecasting step; \mathbf{D} is the matrix of measurement data perturbed by noise, of dimensions $m \times N$; \mathbf{d}^i is a vector of perturbed measurements; \mathbf{d}^* is the vector of real measurements; and $\boldsymbol{\varepsilon}_i$ is a vector of measurement errors added to the real measurements in order to create perturbed measurements. Each element in the error vector $\boldsymbol{\varepsilon}_i$ is randomly selected from a normal distribution with a zero mean and a variance defined by the input measurement error. Here, \mathbf{R} is a matrix based on $\boldsymbol{\varepsilon}_i$, that is,

$$\begin{aligned} \mathbf{R} &= \frac{\mathbf{e}\mathbf{e}^T}{N-1}, \\ \mathbf{e} &= (\boldsymbol{\varepsilon}_1, \boldsymbol{\varepsilon}_2, \dots, \boldsymbol{\varepsilon}_N). \end{aligned} \quad (9)$$

Also, with reference to equation (3), \mathbf{H} is the measurement operator which relates the state vector to the measurement points; it is in the form of $\mathbf{H} = [\mathbf{0} \mid \mathbf{I}]$, where $\mathbf{0}$ is an $m \times n$ null matrix and \mathbf{I} is an $m \times m$ identity matrix. \mathbf{K}_G is the Kalman gain derived from the minimization of the posterior error covariance of the ensemble of state vectors, that is,

$$\begin{aligned} \mathbf{K}_G &= \mathbf{P}_t^f \mathbf{H}^T (\mathbf{H} \mathbf{P}_t^f \mathbf{H}^T + \mathbf{R})^{-1}, \\ \mathbf{P}_t^f &= \frac{1}{N} (\mathbf{Z}_t^f - \bar{\mathbf{Z}}_t^f) (\mathbf{Z}_t^f - \bar{\mathbf{Z}}_t^f)^T, \end{aligned} \quad (10)$$

where \mathbf{P}_t^f is the error covariance matrix of the ensemble of forecasted state vectors and $\bar{\mathbf{Z}}_t^f$ is the ensemble mean of \mathbf{Z}_t^f , that is,

$$\bar{\mathbf{Z}}_t^f = \mathbf{Z}_t^f \mathbf{1}_N, \quad (11)$$

where $\mathbf{1}_N$ is a matrix in which each element is equal to $1/N$.

At the end of the iteration process, the ensemble mean is considered to be the best estimate of the elastic modulus field, and the soil displacement field can then be updated based on the best estimation.

It is worth noting that kriging can also be used to interpolate the soil responses such as displacements to produce a kriged displacement field. However, the displacement monitoring points are often not intensive enough to allow an accurate estimation of the covariance between displacements

at different points. This form of conditioning is not pursued in this study.

4. Methodology: The Random Finite Element Method

The random finite element method (RFEM) is used to compute the geotechnical structure (e.g., soil excavation) response (e.g., displacement) within a Monte Carlo framework [9]. The procedure is as follows:

- (1) Generate random property fields (either conditional or unconditional), for example, using the local average subdivision (LAS) method [21] (combined with kriging for conditional fields), based on the soil property statistics, e.g., mean, standard deviation, and spatial correlation structure (type of correlation function and horizontal and vertical scales of fluctuation, θ_h and θ_v , respectively);
- (2) Map (conditional or unconditional) random field cell values onto the finite elements within the finite element mesh modelling the given problem (in this case, a soil excavation problem);
- (3) Carry out a traditional finite element (FE) analysis (e.g., staged excavation) [22];
- (4) Repeat the aforementioned steps for multiple realisations in a Monte Carlo analysis (e.g., the number of realisations $N_{mc} = 1000$ in this case) until the output statistics (e.g., mean and standard deviation of the soil displacement) converge.

For a given set of statistics, a probability distribution of the displacement response can be obtained.

An existing finite element program [22] capable of simulating sequential soil excavation is used in this investigation. The excavation is simulated by the removal of elements and the application of forces thus generated to the new boundary. The boundary forces at the i th stage of an excavation are given by

$$F_i = \int_V \mathbf{B}^T \boldsymbol{\sigma}_{i-1} dV - \int_V \mathbf{N}^T \gamma dV, \quad (12)$$

where \mathbf{B} is the strain-displacement matrix, V is the excavated volume, \mathbf{N} is the element shape function, and γ the soil unit weight. The first term is the nodal internal resisting force vector due to the stresses $\boldsymbol{\sigma}$ in the removed elements, and the second term is the reversal of the nodal body-load forces of the removed elements assuming γ (the body-load due to gravity) is acting downwards (negative in this case).

A hypothetical soil excavation problem is considered in this study. Figure 1 shows the finite element mesh of the vertical excavation problem (4 m \times 4 m domain with an element size of 0.5 m \times 0.5 m). The boundary conditions are fixed base and rollers on left and right sides. The meshes used were made up of 8-node quadrilateral elements. Nonlinear elasto-plastic behaviour was assumed with the shear strength defined by a Mohr-Coulomb failure envelope with parameters c and ϕ . A viscoplastic algorithm was used to redistribute the violating stresses in an iterative manner.

Reduced integration was used throughout the mesh. A soil deposit characterised by undrained shear strength $c_u = 9$ kPa was to be excavated in sequence. The unit weight of the soil is $\gamma = 20$ kN/m³, and Poisson's ratio is $\nu = 0.49$. The elastic modulus is assumed to be spatially variable, with a mean of $\mu_E = 1.0 \times 10^5$ kPa, coefficient of variation of $V_E = 0.2$, and an isotropic scale of fluctuation of $\theta = 1$ m. For the present case, the vertical excavation is to occur in 4 steps, leading to a cut of depth 2 m. As can be seen from Figure 1, the first excavation removes elements 5–8, and the second excavation removes elements 13–16 and so on until the fourth excavation. For a vertical cut consisting of undrained clay with a strength of 9 kPa, Taylor [23] predicts a critical height of approximately 1.73 m which is well within the range of the 4th excavation. Twelve inclinometers have been “instrumented on-site” to monitor the displacement field during excavation and these are shown in Figure 1 as well. In order to investigate how the conditional simulation affects the response uncertainties in displacements, a node in the mesh has been selected as the target node to investigate the uncertainty reduction and this is also shown in Figure 1.

Note that LAS has been used to generate 1000 random fields as initial ensemble members. It has also been used to generate a single reference realisation, based on the same statistics as used for the ensemble. This is to represent “real” values of elastic modulus (as might be obtained from the field) and has been used in the FE excavation analysis to produce “real” data of monitored displacements (i.e., at 12 locations) to be assimilated.

Note also that usually soil excavations are supported by structural elements during excavation [24, 25]. This paper, however, investigates the excavation problem without referring to specific supports for simplicity, partly due to the excavation being only 2 m deep. Soil excavation is a typical soil-structure interaction problem where either the soil performance or the structural element performance may be unsatisfactory during excavation. A more realistic analysis considering the performance of both the soil and the structural element is an ongoing research subject for authors (i.e., for deep excavations).

5. Results and Discussion of Conditional Simulation of Soil Excavation

This section presents the results of the conditional simulation of a soil excavation problem stated in the previous section. The results are presented here in three categories, i.e., when direct information or indirect response information is used or when these two sources of information are combined.

5.1. Conditional Simulation via Kriging (Direct Information).

Soil elastic modulus can be measured from laboratory or in situ tests. It can also be estimated based on correlation with other soil properties [26]. In the laboratory, it can be determined from the triaxial test or from the oedometer test (indirectly). On-site, it can be estimated from the standard penetration test (SPT), cone penetration test (CPT),

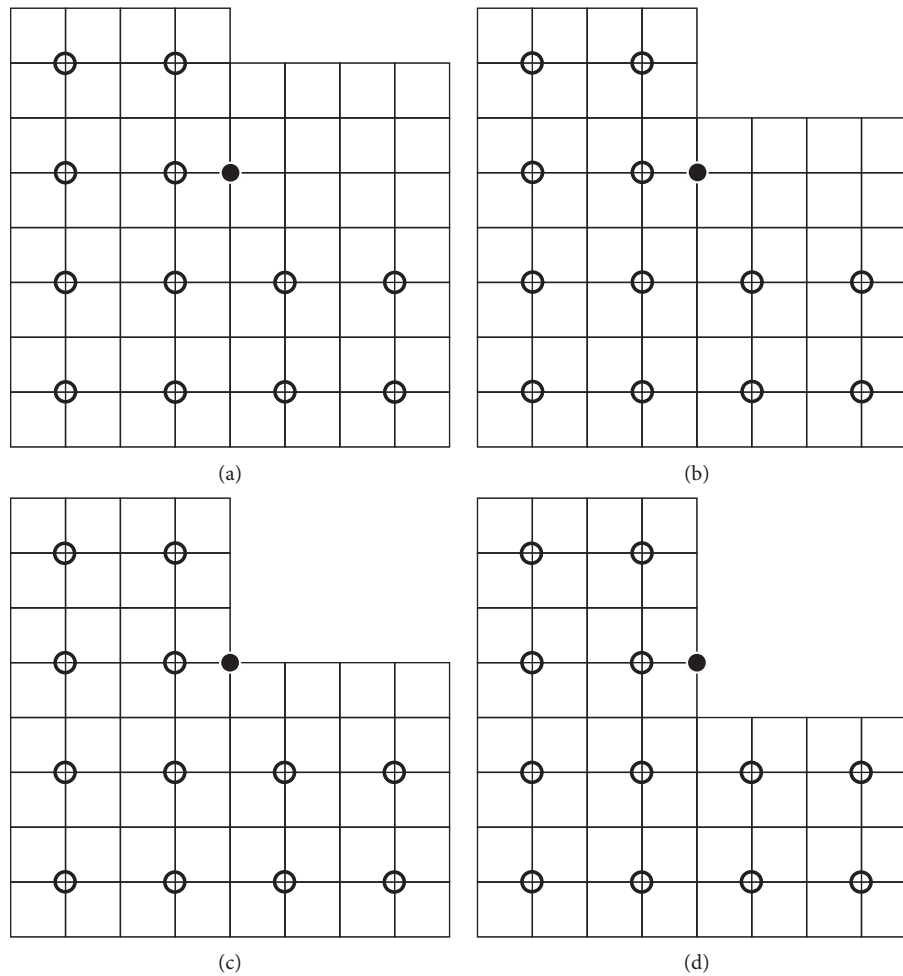


FIGURE 1: Finite element mesh and excavation sequence: 1st layer excavation (a), 2nd layer excavation (b), 3rd layer excavation (c), and 4th layer excavation (d) (circles indicate 12 displacement measurement locations, and the dot indicates the target node where uncertainties in displacements are to be investigated).

pressuremeter test or dilatometer test (indirectly). This paper assumes that the elastic modulus is estimated based on correlation with soil undrained shear strength, which is in turn correlated with CPT measurements. Therefore, known measurements are assumed to be arranged in the form of columns of elements in the following sections, i.e., in the same way as CPTs are taken.

Figures 2 and 3 show two example realisations of the elastic modulus fields, respectively, for the case where one CPT is taken at the second column. In both figures, various fields are presented in the following sequence: an unconditional field, an conditional field, a kriged field based on randomly generated values at measurement locations, and the kriged field based on measurement values. The field values are shown in grey scale, with black cells denoting small values and white cells high values. Also, the two figures use the same global color scale in order to better compare between realisations. It is seen that the variation between realisations reduces upon conditioning, i.e., variations between figures 2(b) and 3(b) are less apparent than variations between figures 2(a) and 3(a). Moreover, the kriged fields are smoother (either based on random values or measurement

values), compared to both conditional and unconditional fields. This highlights the difference between random field simulation and kriging estimation, i.e., random field simulation reproduces the spatial variation of the measured field whereas kriging estimation typically has a smoothing effect on real data.

Similar to Figures 2 and 3, Figures 4 and 5 show two example realisations of the elastic modulus fields, when two CPTs are taken at the 2nd and 7th column, respectively. It is seen that by preserving the measurement values at the 7th column, the updated random fields (Figures 4(b) and 5(b)) become closer to the reference (actual) field (see Figure 6(a)); i.e., those realisations that include unrealistic values in the vicinity of the additional measurements have been updated.

Figures 7(a)–7(f) shows the normalised histograms and fitted probability density functions (PDF) of the horizontal (X) and vertical (Y) displacements of the target point, in the first three consecutive excavation steps, for unconditional simulation and conditional simulation honoring one CPT and two CPTs. It is worth noting that the displacements are relatively small due to the use of a large mean elastic modulus. The dashed vertical line in the figure represents the

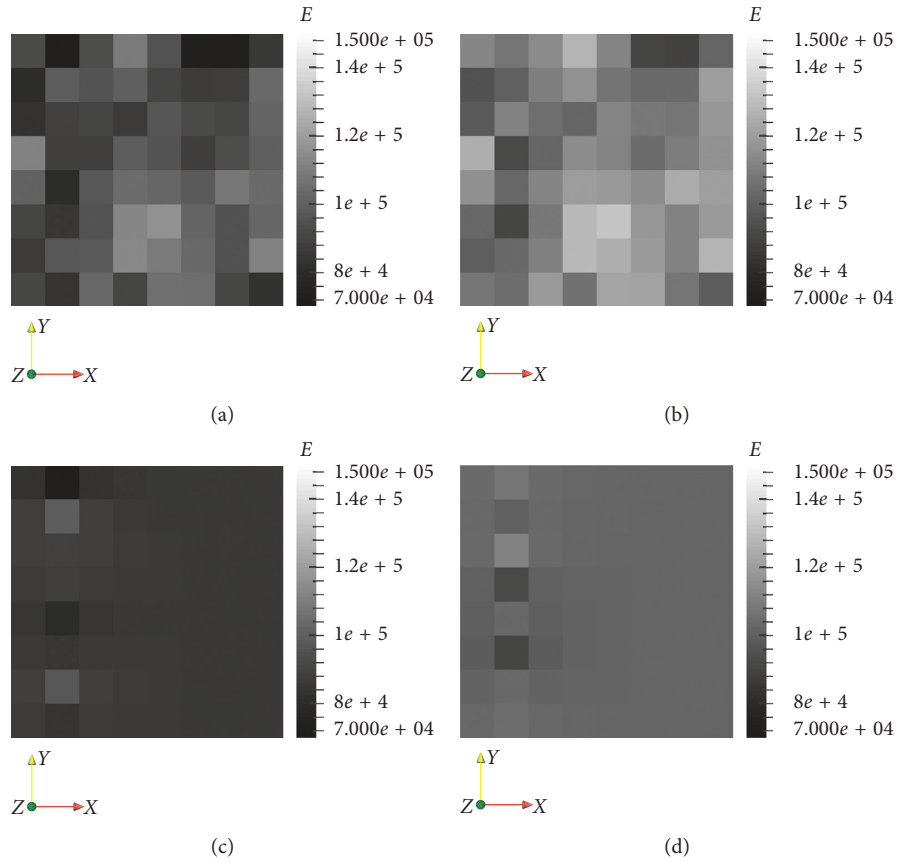


FIGURE 2: Example realisation i for unconditional field (a), conditional field (b), kriged field based on random field values at measurement locations (c), and kriged field based on measurement values (d), 1 CPT.

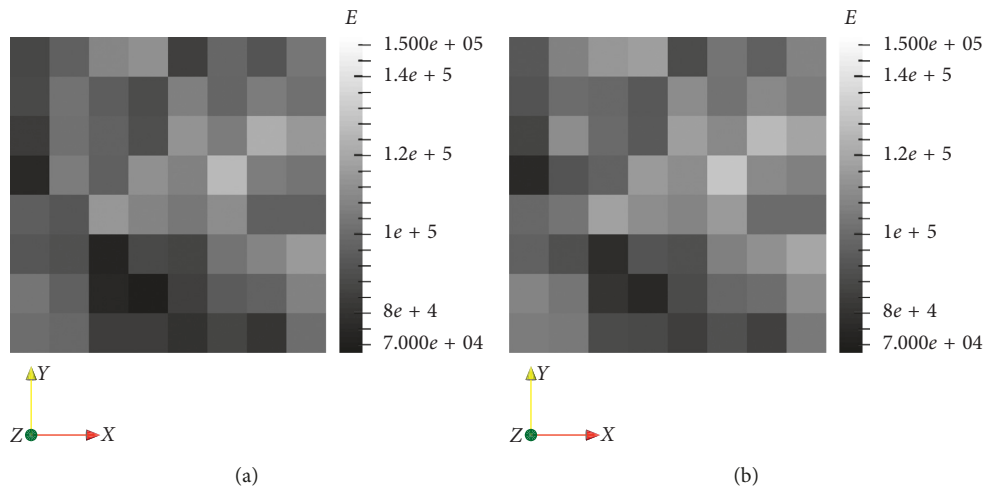


FIGURE 3: Continued.

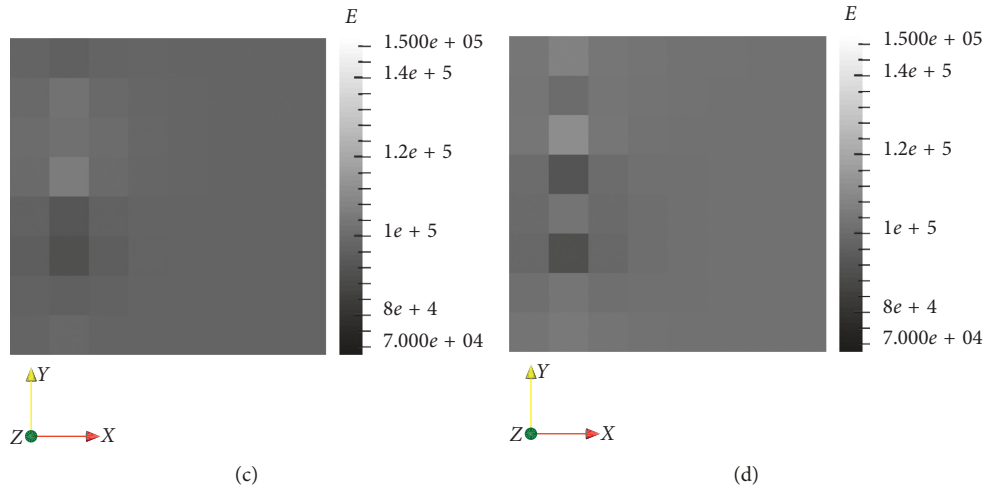


FIGURE 3: Example realization j for unconditional field (a), conditional field (b), kriged field based on random field values at measurement locations (c), and kriged field based on measurement values (d), 1 CPT.

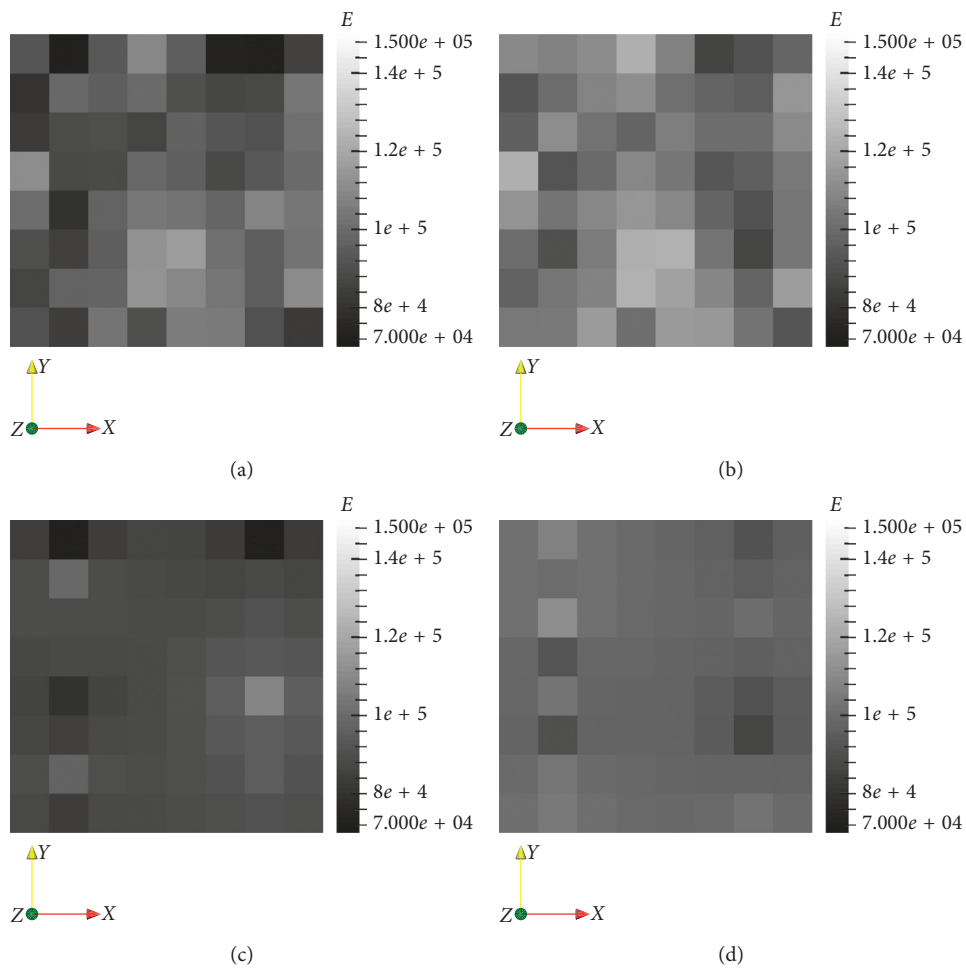


FIGURE 4: Example realization i for unconditional field (a), conditional field (b), kriged field based on random field values at measurement locations (c), and kriged field based on measurement values (d), 2 CPTs.

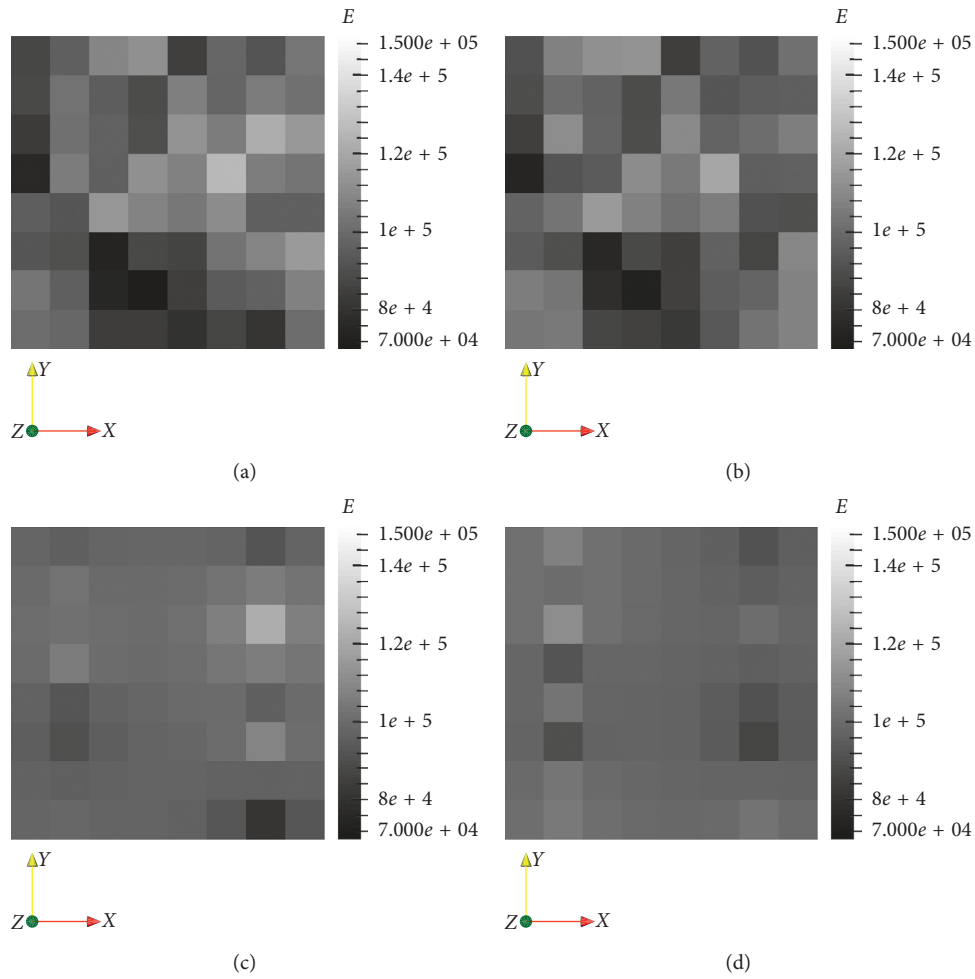


FIGURE 5: Example realisation j for unconditional field (a), conditional field (b), kriged field based on random field values at measurement locations (c), and kriged field based on measurement values (d), 2 CPTs.

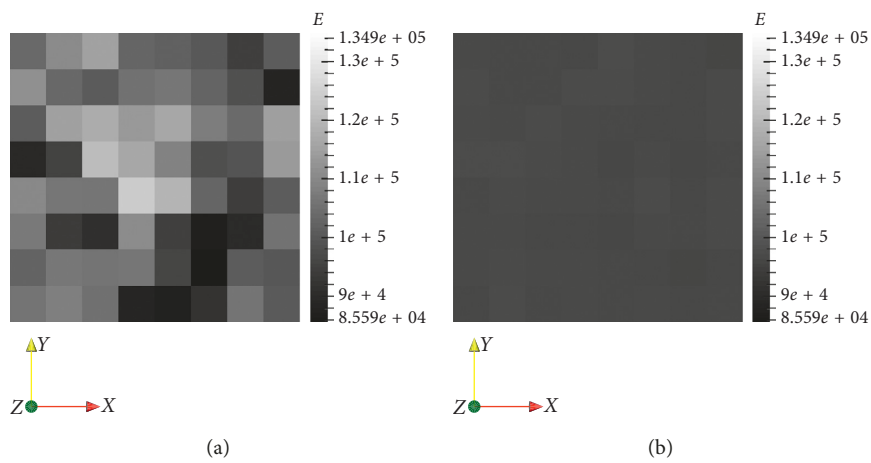


FIGURE 6: Continued.

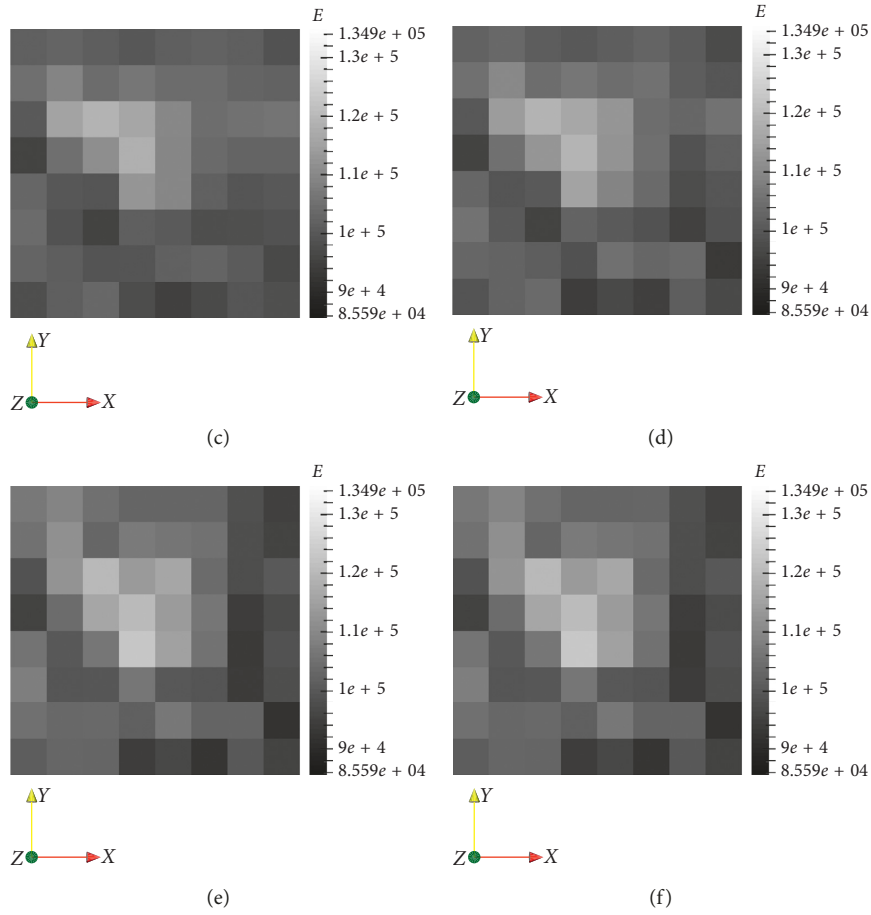


FIGURE 6: Reference field (a), initial estimation (i.e., ensemble mean) (b), updated estimation after excavating the 1st layer (c), updated estimation after excavating the 2nd layer (d), updated estimation after excavating the 3rd layer (e), and updated estimation after excavating the 4th layer (f).

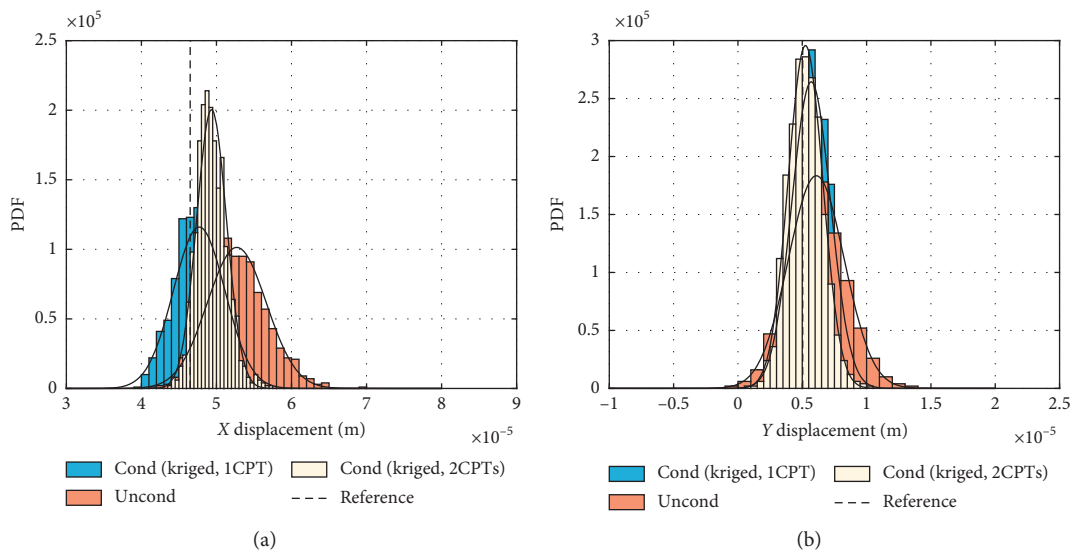


FIGURE 7: Continued.

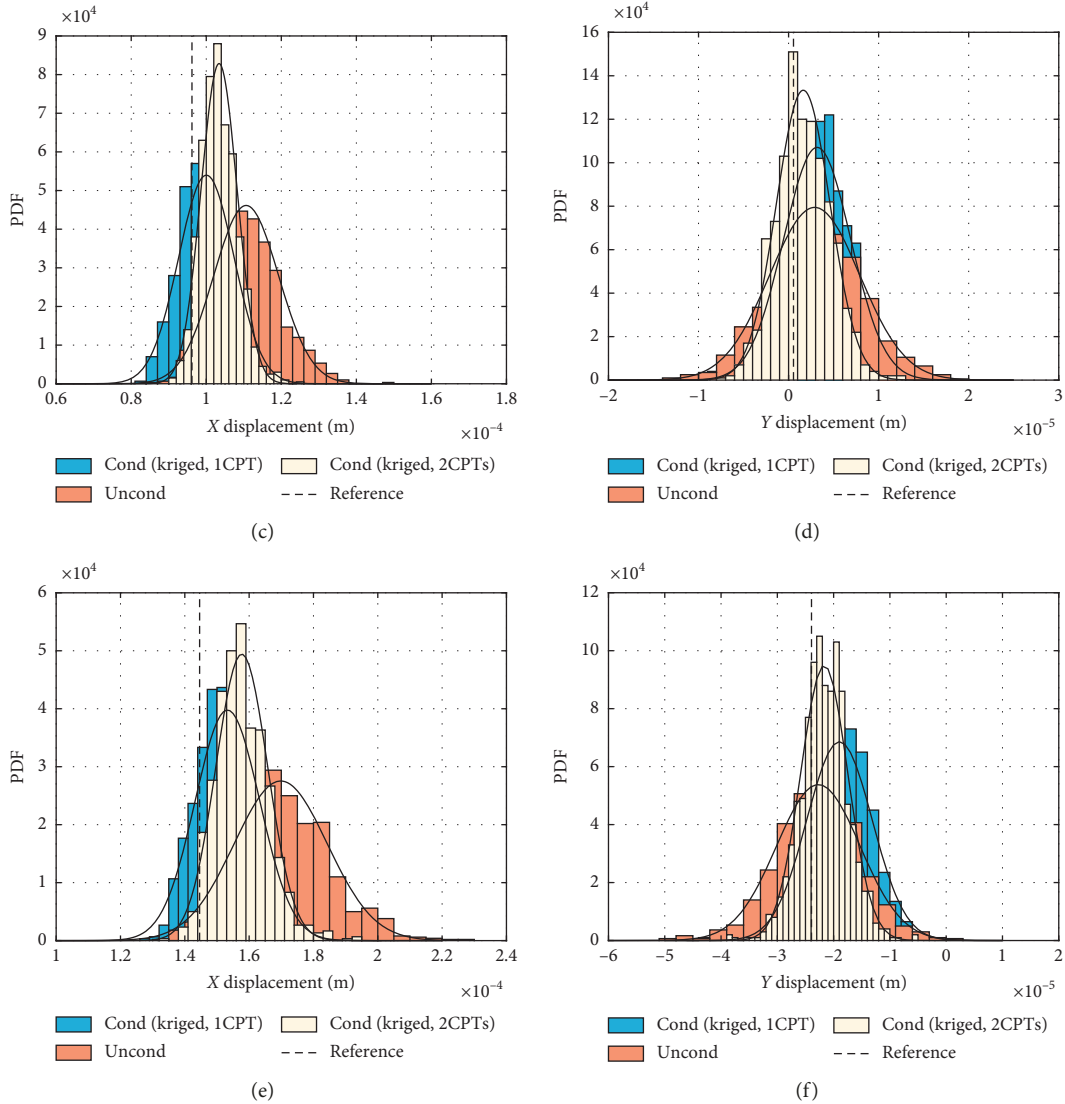


FIGURE 7: PDF of target point displacements in excavation steps 1–3: comparison between unconditional simulation and conditional simulation based on 1 CPT measurement and 2 CPT measurements. (a) First layer excavation (X), (b) first layer excavation (Y), (c) second layer excavation (X), (d) second layer excavation (Y), (e) third layer excavation (X), and (f) third layer excavation (Y).

reference value, that is, the FE analysis calculated value based on the reference field. It is seen that the uncertainties in the displacements reduce as a result of including the measurement values in the elastic modulus field. Moreover, the uncertainty reduction (i.e., as indicated by the decreasing standard deviation of the probability distribution) when considering two CPTs is larger compared to that when considering only one CPT. In order to quantify the uncertainty reduction, a performance-based uncertainty reduction ratio is defined as

$$u_d^i = \sigma_{\text{cond}}^i / \sigma_{\text{uncond}}^i, \quad (13)$$

where σ_{cond}^i and σ_{uncond}^i denote the standard deviation of the probability distribution of the i th step X or Y displacements of the target points in the conditional and unconditional simulation, respectively. In this case, $u_d^1 = 0.8739$ for 1 CPT

conditioning and $u_d^1 = 0.5060$ for 2 CPTs when assessing the uncertainties in the 1st step X displacement of the target point. The uncertainty reduction ratios of the X and Y displacements in the three excavation steps are shown in Tables 1 and 2, respectively.

5.2. Conditional Simulation via EnKF (Indirect Information).

The measured responses, i.e., displacements, are used in this section to investigate the effect of the inclusion of such indirect information on the probability distributions of the excavation displacements. To facilitate understanding, a flowchart in the case of a soil excavation problem is shown in Figure 8. Similar to the previous section, probability updating is presented specifically for the target point, although the analysis has more or less the same effect on other node points.

TABLE 1: Uncertainty reduction ratio u_d^i in X displacements.

Excavation step	Conditional 1 CPT	Conditional 2 CPTs	Conditional EnKF	Conditional 1 CPT + EnKF	Conditional 2 CPTs + EnKF
1	0.8739	0.5060	—	—	—
2	0.8548	0.5568	0.4861	0.4085	0.2640
3	0.6921	0.5571	0.3368	0.2520	0.1827

TABLE 2: Uncertainty reduction ratio u_d^i in Y displacements.

Excavation step	Conditional 1 CPT	Conditional 2 CPTs	Conditional EnKF	Conditional 1 CPT + EnKF	Conditional 2 CPTs + EnKF
1	0.6936	0.6202	—	—	—
2	0.7244	0.5958	0.6106	0.4592	0.3914
3	0.7846	0.5669	0.4907	0.3757	0.3492

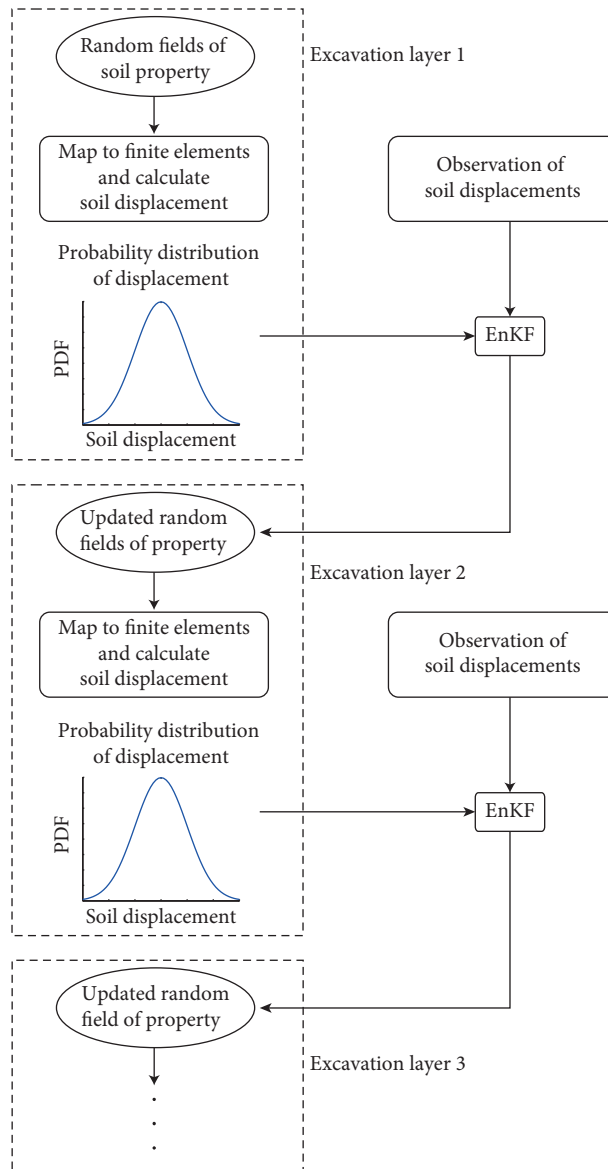


FIGURE 8: Flowchart of the conditional simulation via EnKF.

In order to reduce the uncertainties in the displacement responses, the inverse modelling technique EnKF is used. Figure 6 shows the initial estimation of the field

when there are no displacement measurements and the updated field estimation after 4 excavation layers, respectively. The reference field is also shown in the figure. It

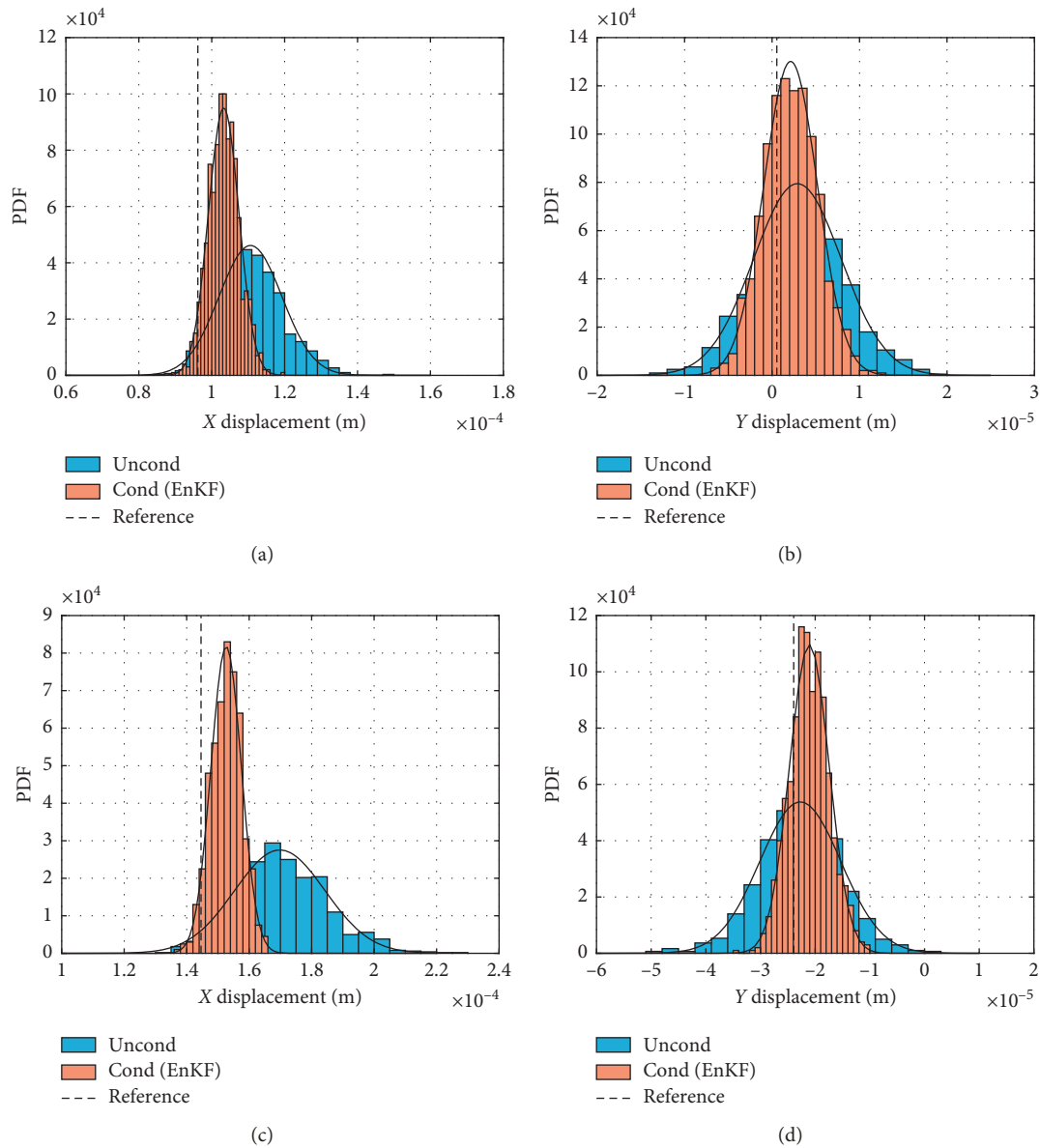


FIGURE 9: PDF of target point displacements in excavation steps 2-3: comparison between unconditional simulation and conditional simulation based on displacement measurements. (a) Second layer excavation (X), (b) second layer excavation (Y), (c) third layer excavation (X), and (d) third layer excavation (Y).

is seen that after the first excavation step, the field estimation starts to improve. After the second excavation layer, the field estimation is closer to the reference field. The field resembles the reference field after the 3rd and 4th excavation layer.

Figure 9 shows the effect of updating the elastic modulus field on the probability distributions of the target point displacements in the 2nd and 3rd excavation steps, respectively. It is seen that the conditional simulation via EnKF reduces the displacement variation, i.e., it reduces the variance of the distribution. The distribution moves closer to the reference values that are obtained from the reference field. Also, a comparison with previous conditional simulation results (i.e., Figures 7(c)–7(f) and Tables 1 and 2) indicates that conditional simulation via EnKF has a larger

effect on the uncertainty reduction than conditional simulation via kriging 1 CPT measurement (at the 2nd column in this case), although the differences are smaller for conditional simulation via kriging 2 CPTs. Note that the relative effect of EnKF and kriging may change for a different case. It is a function of a number of factors including the number and relative arrangement of displacement monitoring points and the number and relative positioning of direct measurements (e.g., CPT).

5.3. Conditional Simulation via Both Kriging and EnKF. The two techniques have been combined in this section to investigate the effect on the excavation problem, as more often both direct measurements and indirect monitoring

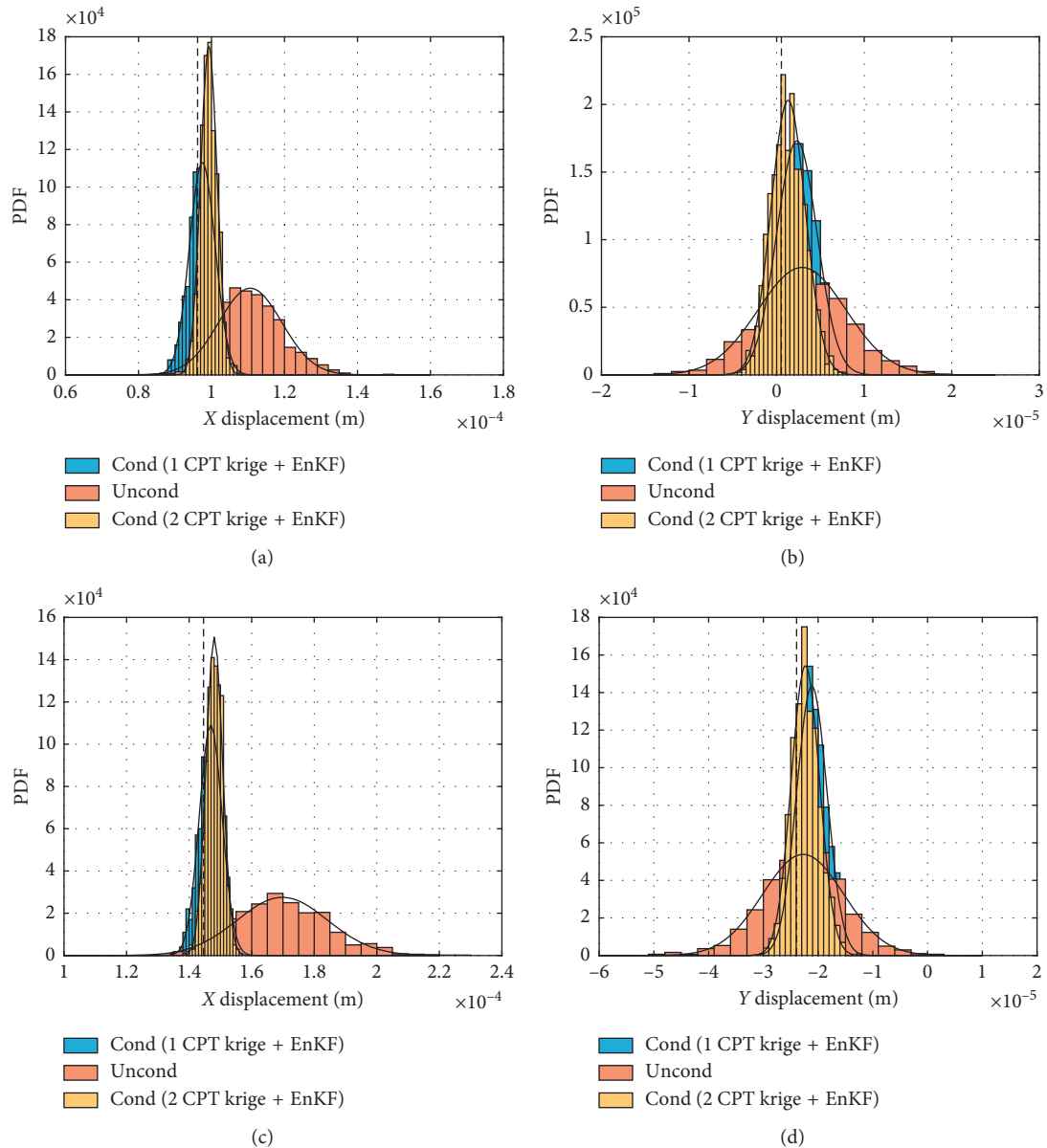


FIGURE 10: PDF of target point displacements in excavation steps 2-3: comparison between unconditional simulation and conditional simulation based on CPT and displacement measurements. (a) Second layer excavation (X), (b) second layer excavation (Y), (c) third layer excavation (X), and (d) third layer excavation (Y).

data are available. Figure 10 shows PDFs of displacement responses of the target point for the unconditional simulation, the conditional simulation via EnKF and kriging 1 CPT, and the conditional simulation via EnKF and kriging 2 CPTs. In contrast to EnKF (Figure 9) or kriging (Figure 7) alone, combining EnKF and kriging produces a probability distribution that is narrower and closer to the reference value. The uncertainty reduction ratios shown in Tables 1 and 2 clearly demonstrate this effect.

6. Conclusions

The paper presents a framework to reduce uncertainty in soil spatial variability and thus in soil structure performance through conditional simulation of the soil property field, by making use

of either the direct measurement data or the indirect response monitoring data. A hypothetical soil excavation example is used to demonstrate the updating of the probability distributions of soil displacement in the series of excavation steps.

It is first shown that conditional simulation based on direct measurements can reduce the range of possible field realisations and therefore the uncertainty (indicated by the variance of the probability distribution) in the displacement responses. Then it is illustrated that the EnKF can be used efficiently to improve the knowledge on the soil property field (i.e., soil elastic modulus in this case) and on the displacement probability of the excavation pit. It is found that in the present study, the EnKF is more efficient in reducing the displacement uncertainty than kriging only one CPT test. Although increasing the number of direct CPT

measurements reduces the difference between the two, the conditional simulation based on EnKF is still more efficient in most cases. However, the performance of the two conditional simulations is believed to be dependent on the arrangement and number of direct measurement points and indirect monitoring points and the degree of spatial variability (i.e., the spatial fluctuation scale of the soil property in the ground).

Nevertheless, the results show that conditional simulation that makes use of all the available data (i.e., direct and indirect) can more effectively improve the prediction of soil displacements than conditional simulation that takes advantage of either one source of data. Moreover, EnKF can be effectively used to sequentially update the property field, following the excavation sequence. The implication is that this updating process can be continued step by step to direct and refine the construction process.

Data Availability

The data used to support the findings of this study are available from the corresponding author upon request.

Conflicts of Interest

The authors declare that they have no conflicts of interest.

Acknowledgments

The first author appreciates the financial support of the National Natural Science Foundation of China (grant no. 41807228) and the Fundamental Research Funds for the Central Universities (grant no. 2652017071), and the second author appreciates the financial support of the National Natural Science Foundation of China (grant no. 51908175).

References

- [1] K. K. Phoon and F. H. Kulhawy, "Characterization of geotechnical variability," *Canadian Geotechnical Journal*, vol. 36, no. 4, pp. 612–624, 1999.
- [2] Y. J. Li, *Reliability of long heterogeneous slopes in 3D- model performance and conditional simulation*, Ph.D. thesis, Delft University of Technology, Delft, Netherlands, 2017.
- [3] M. A. Hicks and Y. Li, "Influence of length effect on embankment slope reliability in 3D," *International Journal for Numerical and Analytical Methods in Geomechanics*, vol. 42, no. 7, pp. 891–915, 2018.
- [4] X. Y. Li, L. M. Zhang, and J. H. Li, "Using conditioned random field to characterize the variability of geologic profiles," *Journal of Geotechnical and Geoenvironmental Engineering*, vol. 142, no. 4, Article ID 04015096, 2015.
- [5] Y. J. Li, M. A. Hicks, and P. J. Vardon, "Uncertainty reduction and sampling efficiency in slope designs using 3D conditional random fields," *Computers and Geotechnics*, vol. 79, pp. 159–172, 2016.
- [6] D. G. Krige, "A statistical approach to some mine valuation and allied problems on the witwatersrand," M.S. thesis, University of the Witwatersrand, Johannesburg, Gauteng, South Africa, 1951.
- [7] M. K. Lo and A. Y. Leung, "Bayesian updating of subsurface spatial variability for improved prediction of braced excavation response," *Canadian Geotechnical Journal*, vol. 56, no. 8, pp. 1169–1183, 2018.
- [8] P. J. Vardon, K. Liu, and M. A. Hicks, "Reduction of slope stability uncertainty based on hydraulic measurement via inverse analysis," *Georisk: Assessment and Management of Risk for Engineered Systems and Geohazards*, vol. 10, no. 3, pp. 223–240, 2016.
- [9] G. A. Fenton and D. V. Griffiths, *Risk Assessment in Geotechnical Engineering*, John Wiley & Sons, New York, NY, USA, 2008.
- [10] C. C. Li and A. Der Kiureghian, "Optimal discretization of random fields," *Journal of Engineering Mechanics*, vol. 119, no. 6, pp. 1136–1154, 1993.
- [11] H. G. Matthies, C. E. Brenner, C. G. Bucher, and C. Guedes Soares, "Uncertainties in probabilistic numerical analysis of structures and solids-stochastic finite elements," *Structural Safety*, vol. 19, no. 3, pp. 283–336, 1997.
- [12] A. Der Kiureghian and J. B. Ke, "The stochastic finite element method in structural reliability," in *Stochastic Structural Mechanics*, pp. 84–109, Springer, New York, NY, USA, 1987.
- [13] E. Vanmarcke and M. Grigoriu, "Stochastic finite element analysis of simple beams," *Journal of Engineering Mechanics*, vol. 109, no. 5, pp. 1203–1214, 1983.
- [14] W. K. Liu, T. Belytschko, and A. Mani, "Random field finite elements," *International Journal for Numerical Methods in Engineering*, vol. 23, no. 10, pp. 1831–1845, 1986.
- [15] K. K. Phoon, S. P. Huang, and S. T. Quek, "Simulation of second-order processes using Karhunen-Loeve expansion," *Computers & Structures*, vol. 80, no. 12, pp. 1049–1060, 2002.
- [16] E. H. Vanmarcke, "Probabilistic characterization of soil profiles," in *Site Characterization & Exploration*, pp. 199–219, ASCE, Evanston, Illinois, USA, 1978.
- [17] M. A. Hicks and K. Samy, "Influence of heterogeneity on undrained clay slope stability," *Quarterly Journal of Engineering Geology and Hydrogeology*, vol. 35, no. 1, pp. 41–49, 2002.
- [18] M. A. Hicks and W. A. Spencer, "Influence of heterogeneity on the reliability and failure of a long 3D slope," *Computers and Geotechnics*, vol. 37, no. 7–8, pp. 948–955, 2010.
- [19] Y. J. Li, M. A. Hicks, and J. D. Nuttall, "Comparative analyses of slope reliability in 3D," *Engineering Geology*, vol. 196, pp. 12–23, 2015.
- [20] G. A. Fenton, "Error evaluation of three random-field generators," *Journal of Engineering Mechanics*, vol. 120, no. 12, pp. 2478–2497, 1994.
- [21] G. A. Fenton and E. H. Vanmarcke, "Simulation of random fields via local average subdivision," *Journal of Engineering Mechanics*, vol. 116, no. 8, pp. 1733–1749, 1990.
- [22] I. M. Smith and D. V. Griffiths, *Programming the Finite Element Method*, John Wiley & Sons, New York, NY, USA, 2005.
- [23] D. W. Taylor, "Stability of earth slopes," *Journal of the Boston Society of Civil Engineers*, vol. 24, pp. 197–246, 1937.
- [24] Z. Luo, S. Atamturktur, C. H. Juang, H. Huang, and P. S. Lin, "Probability of serviceability failure in a braced excavation in a spatially random field: fuzzy finite element approach," *Computers and Geotechnics*, vol. 38, no. 8, pp. 1031–1040, 2011.
- [25] W. Gong, C. Juang, and J. Martin, "A new framework for probabilistic analysis of the performance of a supported excavation in clay considering spatial variability," *Géotechnique*, vol. 67, pp. 546–552, 2016.
- [26] K.-K. Phoon and F. H. Kulhawy, "Evaluation of geotechnical property variability," *Canadian Geotechnical Journal*, vol. 36, no. 4, pp. 625–639, 1999.

